RSC Advances

PAPER

View Article Online
View Journal | View Issue

Cite this: *RSC Adv.*, 2020, **10**, 35480

A new environmentally-friendly route to *in situ* form a high-corrosion-resistant nesquehonite film on pure magnesium

Xianlong Cao, *[abc] Quanyou Ren,[b] Youkun Yang,[b] Xianglong Hou,[b] Yongbo Yan,[b] Jie Hu,[b] Hongda Deng,[b] Daliang Yu,[b] Wei Lan[b] and Fusheng Pan[ac]

Magnesium-based materials are promising lightweight structural materials due to their excellent properties. However, their extensive application has been severely limited due to their high corrosion susceptibility. The inadequate corrosion resistance of Mg is mainly attributed to the porous and unprotective native surface film formed on Mg in aggressive environments. Here, we demonstrated a new environment-friendly route for the growth of a continuous nesquehonite ($MgCO_3 \cdot 3H_2O$) protective film on the surface of pure Mg metal at a relatively low temperature *via* an *in situ* reaction of the Mg surface with gaseous phase CO_2 in humid environments. The protective film consists solely of highly crystalline $MgCO_3 \cdot 3H_2O$ that is compact and has an umbrella-like structure. Electrochemical tests showed that compared to the untreated Mg substrate, the protective film can effectively improve the corrosion resistance of the substrate by nearly two orders of magnitude. Additionally, a possible formation mechanism of the nesquehonite film on the pure Mg was proposed and the effect of the carbonation time on the film was investigated. This environmentally-friendly surface treatment method is promising for use in the protection of magnesium-based materials.

Received 18th May 2020
Accepted 15th September 2020

DOI: 10.1039/d0ra04423g

rsc.li/rsc-advances

1 Introduction

Because of the low weight and energy-saving and environmentally-friendly characteristics of Mg, magnesium (Mg)-based materials are desirable in many engineering applications including in transportation, 3C products, medical biomaterials, and in the aerospace industry.[1,2] However, Mg-based materials are also the most reactive of all engineering materials and their inadequate corrosion resistance severely restricts their wide application in many service conditions, particularly in chloride-containing media. This corrosion is primarily attributed to the high thermodynamic activity of Mg and the lack of the protective effect of the oxide film on the Mg surface[2,3] and has severely decreased the application potential of Mg-based materials. In the past several decades, many efforts have been carried out to improve the corrosion resistance of magnesium-based materials.[3–5] In particular, creation of a surface film that can act as a barrier to protect the Mg substrate from attack by the aggressive service environment is a widely applied strategy for preventing Mg metal corrosion.[6] The frequently used surface treatment techniques include chemical conversion films, thermal spray coating, electroplating, electroless plating, anodic/micro-arc oxidation, and organic coating.[5,6] Unfortunately, the above-mentioned methods unavoidably produce some highly toxic chemical waste, contradicting the original purpose of the use of Mg metal as a green engineering material. Considering the huge demand for Mg-based materials, it is imperative to develop environmentally-benign Mg surface protection methods.

Recently, the carbonation method has emerged an attractive and promising method for the corrosion protection of Mg metal.[2,7,8] Through reaction with the CO_2 excited by either a high-energy electron beam or a glow discharge, Wang *et al.*[2,7] carbonated an Mg-based material to create a smooth and dense magnesium carbonate protective film. The inhibition effects of this protective film are superior to those of the anodized coating, and the inhibition performance can be even be as good as that of a micro-arc oxidation coating. Sun *et al.*[8] also investigated the interaction between excited CO_2 and Mg substrate under electron beam irradiation and observed a rapid and unique oscillation sublimation process of the Mg metal at room temperature. However, to date, this carbonation method applied to Mg-based materials must rely on activation by either a high-energy electron beam or a glow discharge. Therefore, it is necessary to develop a more facile carbonation method.

Fortunately, an examination of the literature revealed a possible approach for the development of such a facile

[a]College of Materials Science and Engineering, Chongqing University, Chongqing 400045, China
[b]School of Metallurgy and Materials Engineering, Chongqing University of Science and Technology, Chongqing 401331, China. E-mail: xianlong@cqust.edu.cn
[c]National Engineering Research Center for Magnesium Alloys, Chongqing 400045, China

carbonation method. First, several researchers reported that ambient concentrations of CO_2 can inhibit the atmospheric corrosion of pure Mg and Mg alloys.[9] The inhibition effect of CO_2 is attributed to the formation of slightly soluble Mg hydroxy-carbonates through atmospheric corrosion reactions, providing a somewhat protective film on the Mg surface.[9] In addition, it was reported that a continuous and compact lithium carbonate film can form on the surface of a new Mg–Li alloy due to the reaction of lithium oxide reacted with CO_2 in the air.[10] The carbonate-rich surface film provided considerable inhibition of anodic dissolution kinetics.[10,11] However, the protective lithium carbonate only forms on the alloy with a high content of lithium (>11 wt%). While these results show that carbonation on Mg-based materials can be accomplished by chemical and electrochemical reactions even at ambient temperature and pressure, unfortunately, the films formed under these conditions are usually porous, thin and show poor adherence. Interestingly, we also noticed that a protective iron carbonate ($FeCO_3$) film can form through chemical and electrochemical corrosion reactions on the surface of carbon steel used in oil and gas pipelines or tanks in service in wet CO_2 systems with high pressure and temperature.[12,13] The protective $FeCO_3$ layer can effectively reduce the corrosion rate and prolong the service life of carbon steel.[12,13] Therefore, we hypothesize that the control and application of the conditions similar to those found in the operational environment of carbon steel in oil and gas industry will obtain a better protective film on Mg-based materials.

Motivated by the previous results and our hypothesis, in this work, we for the first time demonstrated a new environmentally-friendly carbonation route for the growth of a nesquehonite ($MgCO_3 \cdot 3H_2O$) protective film on the surface of a pure Mg sample *via* an *in situ* reaction of the Mg surface with medium-pressure gaseous phase CO_2 in humid environments at a relatively low temperature. The possible formation mechanism of this nesquehonite film on the pure Mg surface was also discussed. This carbonation method is facile and green, only involves CO_2 and water, and the CO_2 gas and the formed solution can be easily recycled.

2 Experimental

2.1 Pretreatment of pure magnesium

Test samples were prepared from a pure Mg sample (99.99 wt%). The samples were cut into cylinders with the dimensions of Φ1.8 cm × 1.0 cm and then were ground successively using finer grades of emery papers to 1000 grit, rinsed in deionised water, degreased in alcohol, and dried in cold compressed air.

2.2 Film preparation on pure magnesium

Deionised water (500 mL) was injected into a 5 L high-pressure autoclave (American Cortest, USA) and the pretreated pure Mg was suspended in the autoclave with the Mg samples kept 3–10 cm over the waterline. The autoclave was sealed and high-purity CO_2 (99.99%) was then purged into the autoclave at 40 °C until the pressure reached 6.5 MPa. After carbonation for different times (6, 12, 14 and 16 h) in the autoclave, all of the Mg samples were removed and dried in cold compressed air.

2.3 Surface characterization

The surface morphology and elemental composition of the carbonated sample were examined using a field emission scanning electron microscope (FESEM, JSM-7800F, Japan) coupled with an energy dispersive spectroscopy (EDS) analyser. Prior to cross-sectional backscattering electron SEM observations, the carbonated samples were first embedded into epoxy resin, and then were ground successively using a finer grades of emery papers to 1000 grit, rinsed in deionised water, degreased in alcohol, and dried in cold compressed air. X-ray diffraction patterns were obtained using a SmartLab-9 X-ray diffractometer (Rigaku, Japan) operating at 30 kV and 20 mA. The XRD data were recorded within the 2θ range of 10–80° at a scanning rate of 0.04° per step using Cu Kα radiation.

2.4 Corrosion characterization

All of the electrochemical measurements including the evaluation of open-circuit potential (OCP), potentiodynamic polarization and electrochemical impedance spectra (EIS) were performed with a Parstat 4000 electrochemical workstation (Ametek, USA) connected to a traditional three-electrode configuration with the untreated and treated pure Mg samples with the test area of 1 cm^2 as the working electrode, Ag/AgCl/sat. KCl as the reference electrode, and a large platinum net with the dimensions of 20 × 20 mm^2 as the counter electrode. For EIS, a 10 mV AC perturbation (*vs.* OCP) was applied at different frequencies ranging from 100 kHz to 1 mHz. The potentiodynamic polarization experiments were carried out from −20 mV to +1000 mV (*vs.* OCP) at a scan rate of 1 mV s^{-1}.

3 Results and discussion

3.1 Crystal structure analysis

The XRD diffraction spectra of the untreated and treated pure Mg samples kept in gaseous phase CO_2 for different times are shown in Fig. 1a. Only diffraction peaks of the nesquehonite ($MgCO_3 \cdot 3H_2O$) film and the pure Mg substrate phase peaks are observed in the spectra, and no MgO and $Mg(OH)_2$ were detected in this film. In the 2θ range of 10–50°, all of the diffraction peaks for the obtained film match the standard data for nesquehonite (JCPDS 70-1433).[14] The sharp diffraction peaks in the pattern indicate the good crystallinity of the obtained nesquehonite film. Nesquehonite belongs to the monoclinic system (space group $P21/n$, $Z = 4$) with the lattice parameters $a = 7.701$ Å, $b = 5.365$ Å, $c = 12.126$ Å and $\beta = 90.41°$.[14,15] An ideal nesquehonite crystal morphology is illustrated in Fig. 1b. The XRD results indicate that a highly crystalline nesquehonite film was successfully prepared on the pure Mg surface in gaseous phase CO_2.

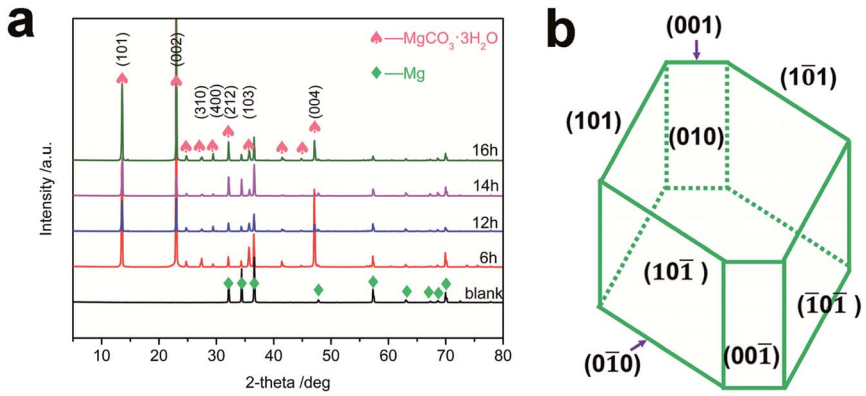

Fig. 1 (a) XRD pattern of the pure Mg substrate and carbonated pure Mg samples kept in gaseous phase CO_2 for different times, and (b) ideal nesquehonite crystal morphology.

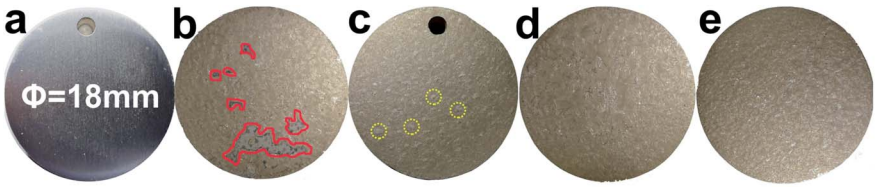

Fig. 2 Macro-morphologies of the untreated (a) and carbonated pure Mg samples in gaseous phase CO_2 for 6 (b), 12 (c), 14 (d) and 16 h (e).

3.2 Morphology and composition analysis

The macro- and micro-morphologies of the film formed on the pure Mg sample carbonated by 6.5 MPa gaseous phase CO_2 at 40 °C for different times are shown in Fig. 2 and 3, respectively. Fig. 4a–d show the SEM micro-morphologies of the Mg sample carbonated for 12 h in greater detail.

Compared to the macro-morphologies of the untreated sample (Fig. 2a), all of the carbonated samples display a light brown nesquehonite film (Fig. 2b–e). However, the surface of the sample treated for 6 h has not yet been completely covered by the nesquehonite film, showing some defective area with either grey or black colour, as marked by red solid lines in Fig. 1b and 2a. By contrast, when treated for over 12 h, all of the

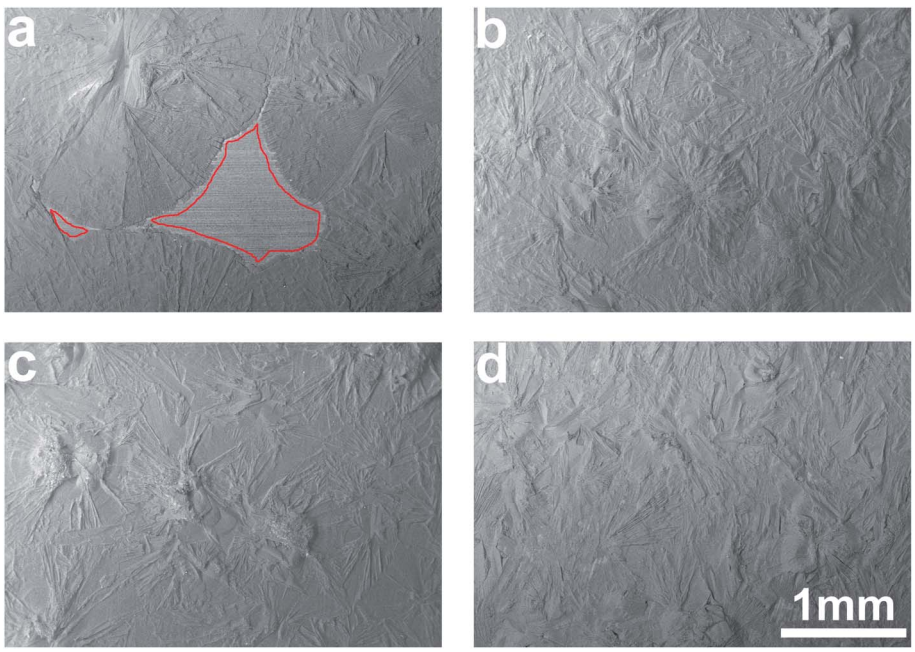

Fig. 3 SEM micrographs of the pure Mg samples carbonated in gaseous phase CO_2 for 6 (a), 12 (b), 14 (c) and 16 h (d).

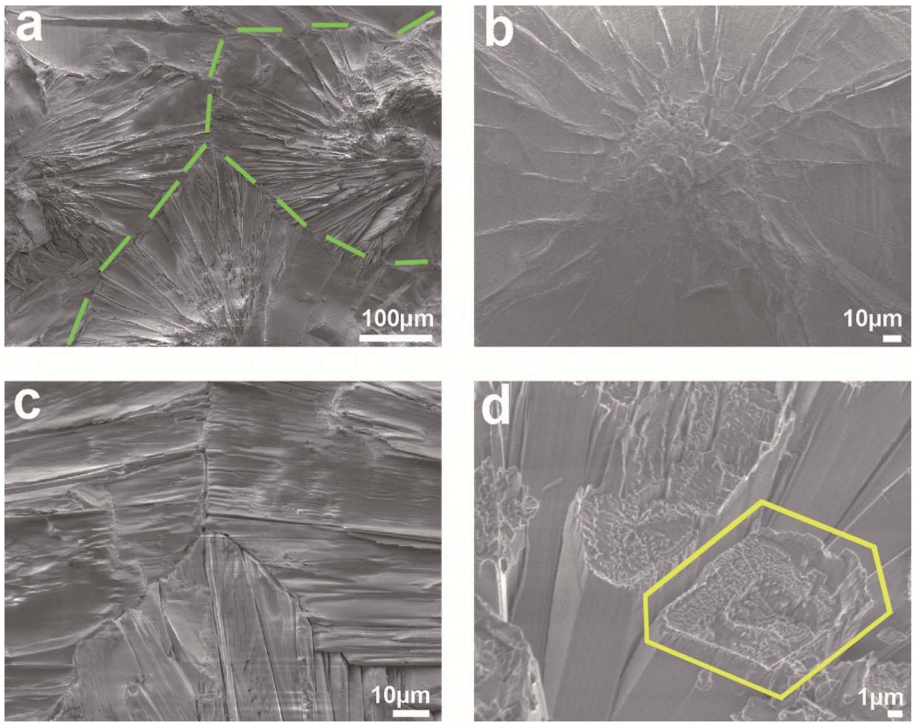

Fig. 4 SEM micrographs of the pure Mg sample carbonated for 12 h: (a) nesquehonite film, (b) centrepiece zone, (c) grain boundary-like zone, (d) single orthorhombic columnar morphology.

Mg samples exhibit a continuous and dense nesquehonite film. In addition, we observed that some small humps are present in the film surface, as marked by yellow circles in Fig. 1c, and the SEM micrographs reveal that nesquehonite film developed around a centrepiece, that is the observed humps, creating an umbrella-like structure covering an area with a diameter of even more than 1 mm (Fig. 3a–d and 4b). These "umbrellas" spread over the pure Mg surface and coalesce along their edges that similar to grain boundaries (green dashed lines) (Fig. 4a and c). From the viewpoint of the centrepiece, the nesquehonite crystals exhibit an apparent orthorhombic cross-section that is consistent with its ideal crystal morphology (Fig. 1b), as marked by yellow solid line in Fig. 4d, and elongate along the c-axis to produce a columnar morphology. Although nesquehonite has an orthorhombic appearance (pseudo-orthorhombic), its symmetry is in fact lower than orthorhombic due to the repeated twinning on the [100] plane and is classified as monoclinic.[16]

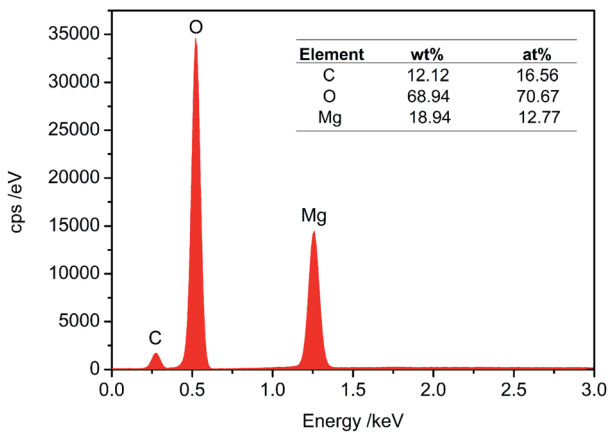

Fig. 5 Surface EDS spectra of the pure Mg alloy carbonated in gaseous phase CO_2 for 12 h.

The composition determined by energy dispersive spectrometer (EDS) spectra for the sample treated for 12 h (Fig. 5) indicates that the film only contains C, Mg and O and no chemical impurities are present. The contents (in wt% and at%) of all of the elements detected by EDS analysis are listed in the inset table in the spectra. It is observed that the C : O : Mg atomic ratio is approximately 1 : 6 : 1 (nominal atomic ratio of $MgCO_3 \cdot 3H_2O$), consistent with the XRD results. EDS mapping shows the existence of Mg, O and C, and their uniform distribution on the Mg surface (Fig. 6), further proving that the formed film is pure nesquehonite.

In addition, a cross-section of the pure Mg sample treated for 12 h was displayed in Fig. 7. Fig. 7a clearly demonstrated that the nesquehonite film has a thickness of 25–150 μm. The film was directly generated on the surface of the pure Mg substrate and was closely attached to the substrate. The cross-section of the film also showed a columnar feature corresponding to the aforementioned umbrella-like structure profile. In particular, the high-magnification images of zones D (Fig. 7c) and E (Fig. 7d) correspond to the "umbrella" edge profile and the "umbrella" centrepiece profile, respectively. The cross-section morphologies further verified the umbrella-like structure with lamination characteristics and revealed the growth direction of

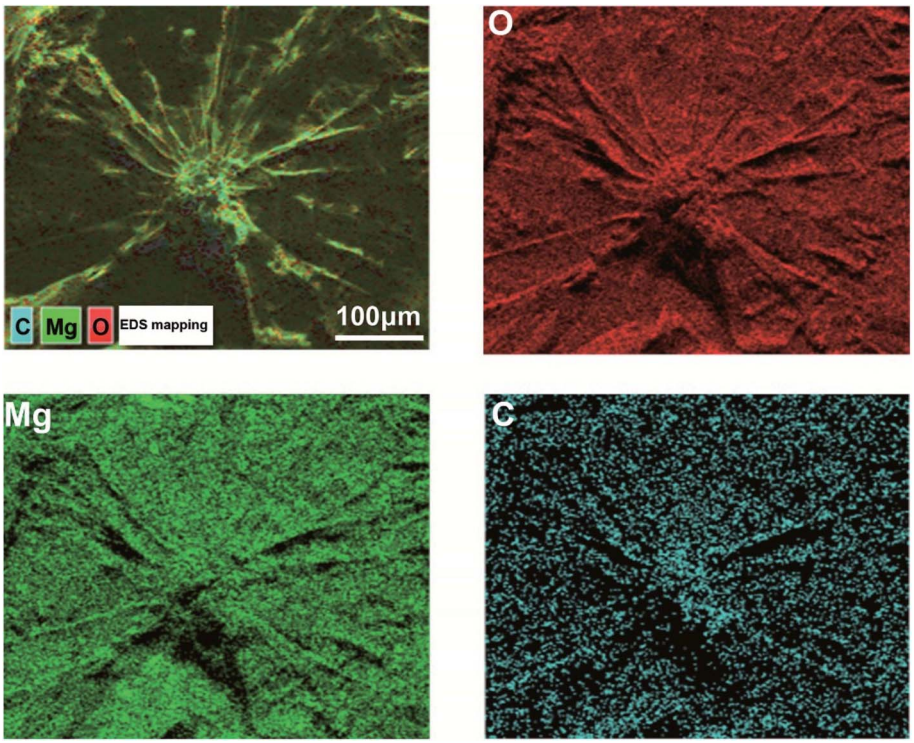

Fig. 6 Surface EDS mapping of the pure Mg carbonated in gaseous phase CO_2 for 12 h.

the film. It is observed that the film showed some interior micro-cracks, which was possibly related to the growth characteristics of the nesquehonite columnar crystal, the CO_2 transport or the release of hydrogen gas during the film formation. The substrate surface beneath the nesquehonite film was clearly uneven, proving the existence of a chemical

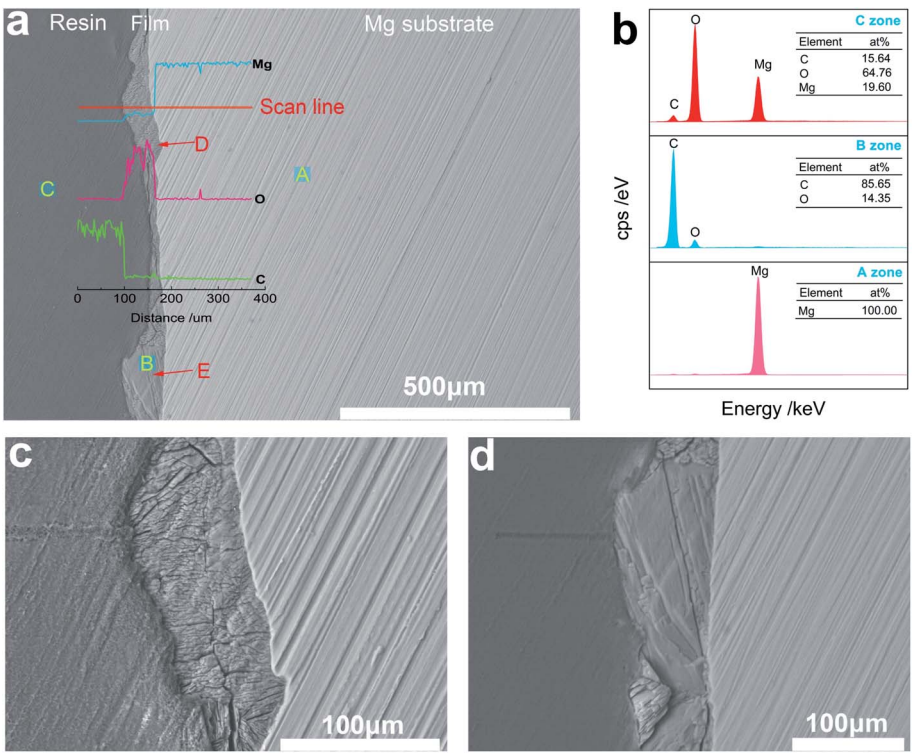

Fig. 7 Cross-sectional observations of the pure Mg carbonated in gaseous phase CO_2 for 12 h: (a) SEM including an inset of the EDS line scan along the red scan line, (b) EDS analysis for zones A, B and C in (a), (c) and (d) magnified view of the selected regions in zones D and E, respectively.

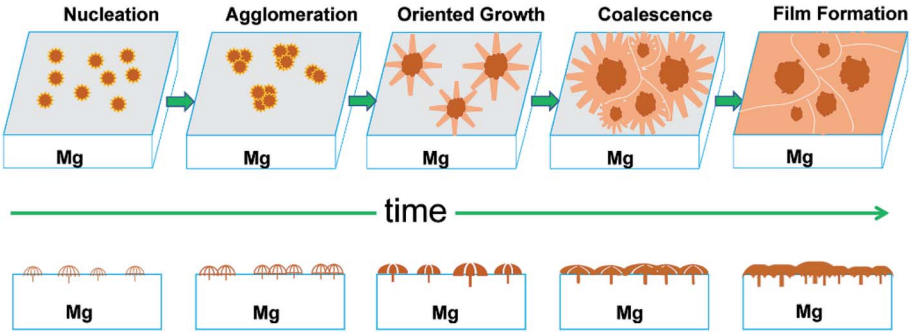

Fig. 8 Proposed formation mechanism of nesquehonite film on the pure Mg substrate.

and/or electrochemical reaction process related to the corrosion dissolution of the substrate during the film formation. The EDS spectra (Fig. 7b) of different zones (A, B and C) and the EDS line scan along the red scan line (Fig. 7a) clearly demonstrate the existence of three distinct zones, that is the Mg substrate, nesquehonite film and resin. For the film zone, three element peaks of Mg, O and C are observed, providing an additional confirmation for the existence of nesquehonite and the formation and possible thickness of the film.

3.3 Proposed film formation mechanism

Our experiments revealed two important findings: (1) no visible film formation was found on the pure Mg surface in the absence of deionised water. (2) Even if the air in the autoclave is exhausted by N_2 flow for 4 h, the film can still form. These two results imply that while oxygen is not necessary, water is critical for the film formation. Based on all of the aforementioned experimental results, the possible reactions involved in the formation process of nesquehonite film on the pure Mg surface are briefly described below.

Upon encountering the evaporated and condensed water molecules adsorbed on the pure Mg surface, CO_2 is hydrated to produce carbonic acid (H_2CO_3):[13]

$$CO_2(g) + H_2O(aq) \leftrightarrow H_2CO_3(aq) \quad (1)$$

that then dissociates in a two-step process described by:

$$H_2CO_3(aq) \leftrightarrow H^+(aq) + HCO_3^-(aq) \quad (2)$$

$$HCO_3^-(aq) \leftrightarrow H^+(aq) + CO_3^{2-}(aq) \quad (3)$$

Localized electrochemical reactions including the hydrogen evolution reaction and electrochemical dissolution of magnesium occur on the Mg surface according to either:[17]

$$Mg(s) \rightarrow Mg^+(aq) + e^- \quad (4)$$

$$2Mg^+(aq) + 2H^+(aq) \rightarrow Mg^{2+}(aq) + H_2\uparrow(g) \quad (5)$$

or

$$2H^+(aq) + 2e^- \rightarrow H_2(g) \quad (6)$$

$$Mg(s) \rightarrow Mg^{2+}(aq) + 2e^- \quad (7)$$

Then, the Mg^{2+} and CO_3^{2-} ions combine to form $MgCO_3 \cdot 3H_2O$ crystal nuclei according to:

$$Mg^{2+}(aq) + CO_3^{2-}(aq) + 3H_2O(aq) \rightarrow MgCO_3 \cdot 3H_2O(s) \quad (8)$$

With the progress of these chemical and electrochemical reactions (reactions 1–8), the $MgCO_3 \cdot 3H_2O$ crystal nuclei increasingly form and a high density of nucleation sites appear. Subsequently, the Mg substrate is gradually covered by tiny crystal grains at an early stage of film formation. Initially, the grains are quite small and their high-index planes are exposed, resulting in the high surface energy of the grain and leading some of the grains to agglomerate and form crystal centrepieces. Once the centrepieces are formed, each single crystal particle in the agglomeration grows according to its own crystal environment, and the oriented growth of the crystal occurs such that the crystal planes with fast growth rate are connected to each other. With increasing reaction time, the further growth of these grains is almost undisturbed until neighbouring grains approach each other. As soon as two as-grown umbrella-like crystals are in close contact with each other, the horizontal growth is terminated, and the between-the-"umbrellas" coalescence proceeds until a continuous and compact nesquehonite film successfully covers the entire surface of the Mg substrate. Fig. 8 illustrates the proposed formation mechanism of the nesquehonite film on the pure Mg substrate.

3.4 Electrochemical corrosion behaviours

3.4.1 Open-circuit potential. When the untreated Mg sample was immersed in the NaCl solution, hydrogen release was observed immediately. The OCP evolution for the untreated sample shows an asymptotical curve towards nobler values during the first 400 s of immersion due to the activation of the Mg substrate (Fig. 9). The initial values are approximately −1.72 V and increase by more than 120 mV, approaching stable values at approximately −1.60 V after 400 s of immersion. This may be attributed to the dissolution of the Mg substrate and the subsequent precipitation of the magnesium hydroxide film ($Mg^{2+} + 2OH^- \rightarrow Mg(OH)_2\downarrow$).[18]

For the carbonated pure Mg samples, the OCP evolution is characterized by a sharp drop during the first 50–200 seconds of immersion (Fig. 9). The OCP reaches a minimum value and then begins to relatively slowly increase towards more positive

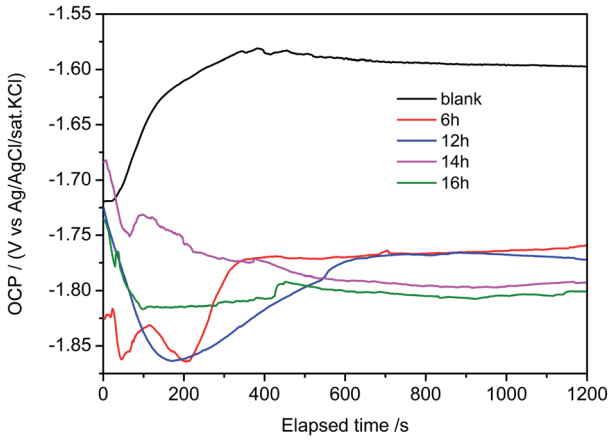

Fig. 9 Open-circuit potential evolution of the untreated and treated pure Mg samples in gaseous phase CO_2 during immersion in 3.5 wt% NaCl solution.

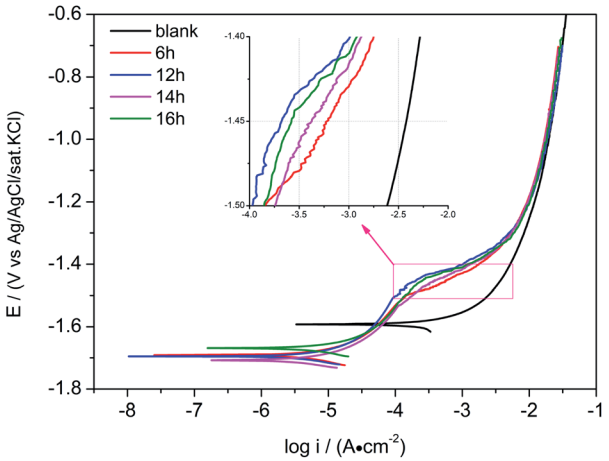

Fig. 10 Potentiodynamic polarization plots of the untreated and treated pure Mg after immersion for 120 min in 3.5 wt% NaCl solution.

values, approaching a stable plateau at approximately −1.75 to −1.81 V after immersion in the 3.5 wt% NaCl solution for 600 s. The drop of the OCP values and their minimum may be related to the cathodic inhibition effect of the nesquehonite film, whereas the rise towards more positive values means that the film starts to gradually become saturated with the NaCl electrolyte. This may be due to the presence of micro-cracks in the interior of the film, and the initiation of the substrate surface oxidation; however, no hydrogen release was observed during the experiment. Furthermore, it is observed from Fig. 9 that the stable OCP plateau becomes more negative with increasing carbonation time. Overall, the OCP evolution indicates that compared to the untreated sample, the nesquehonite film can delay the potential negative shift and provides corrosion protection through a cathodic inhibition mechanism.

3.4.2 Potentiodynamic polarization. The corrosion behaviour of both untreated and treated Mg samples were evaluated by potentiodynamic polarization curves after immersion for 120 min in a 3.5 wt% NaCl solution (Fig. 10). The potentiodynamic polarization curve of the untreated sample displays a high current density due to the dissolution of the pure Mg metal ($Mg \rightarrow Mg^{2+} + 2e^{-}$). A strong anodic activity is also observed with the current density approaching 2.41 mA cm^{-2} for the corrosion potential values that are more negative than −1.50 V. For the carbonated samples, the polarization curves are shifted to the lower corrosion current density area, and the anodic corrosion current density is reduced by nearly two orders of magnitude, indicating that the nesquehonite film is highly effective in preventing the corrosion of the Mg substrate. The anodic corrosion current density of the carbonated Mg samples decreases with longer carbonization time, which may be due to the increasing density of the nesquehonite film. In addition, compared to the untreated substrate, the corrosion potential of the carbonated samples displayed a negative shift of more than 100 mV that can be associated with the cathodic inhibition effects.[18] Thus, the process of cathodic hydrogen release due to the reduction of water occurring on the pure Mg surface ($H_2O + 2e^{-} \rightarrow 2OH^{-} + H_2\uparrow$) was impeded by the nesquehonite film.

Furthermore, we also considered the breakdown potential of the Mg metal in the NaCl solution because it can be used as an indication of the ability of its protective layer to suppress local corrosion destruction.[19] Once the protective layer is broken down through its defective sites, the underlying Mg substrate will be directly exposed to the aggressive environment. While for the untreated Mg sample, no clear breakdown potential is observed, for the carbonated Mg sample, a significant breakdown process of the nesquehonite film is observed from −1.50 V to −1.40 V with an obvious current fluctuation. In particular, for potentials that are more positive than −1.50 V where the current fluctuation is significant (as illustrated in the inset in Fig. 9), the slopes of the anodic branches for all of the carbonated samples decrease, implying that the corrosion becomes easier. When the potential reaches −1.0 V, the anodic branches for all samples completely coincide, indicating that their anodic behaviours are identical for these conditions.

3.4.3 Electrochemical impedance spectroscopy. To further confirm the protective effect of the nesquehonite film, EIS tests were also carried out in 3.5 wt% NaCl, as illustrated in Fig. 9. The EIS Nyquist spectrum (Fig. 11a) and Bode plots (Fig. 11b) of the untreated pure Mg characteristically displays two capacitive loops in the high- and moderate-frequency range and a single inductive loop in the low-frequency range, indicating the presence of three time constants. The capacitive loops are attributed to the either a magnesium hydroxide or oxide film, and the electrochemical double layer at the Mg/electrolyte corroding interface, respectively. The origin of the apparent inductive loop may be attributed to the pitting dissolution of the Mg substrate, the relaxation of adsorbed substance or the peeling off of corrosion products.[20] The EIS Nyquist spectrum (Fig. 11c) and Bode plots (Fig. 11d) of the carbonated samples are characterized by two depressed capacitive loops that imply the presence of two time constants. The capacitive loop in the high-frequency range (10^0 to 10^5 Hz) represents the barrier performance of the nesquehonite protective film formed on the pure Mg surface, while the capacitive loop that appears in the low-frequency range (10^{-2} to 10^0 Hz) corresponds to the response from the

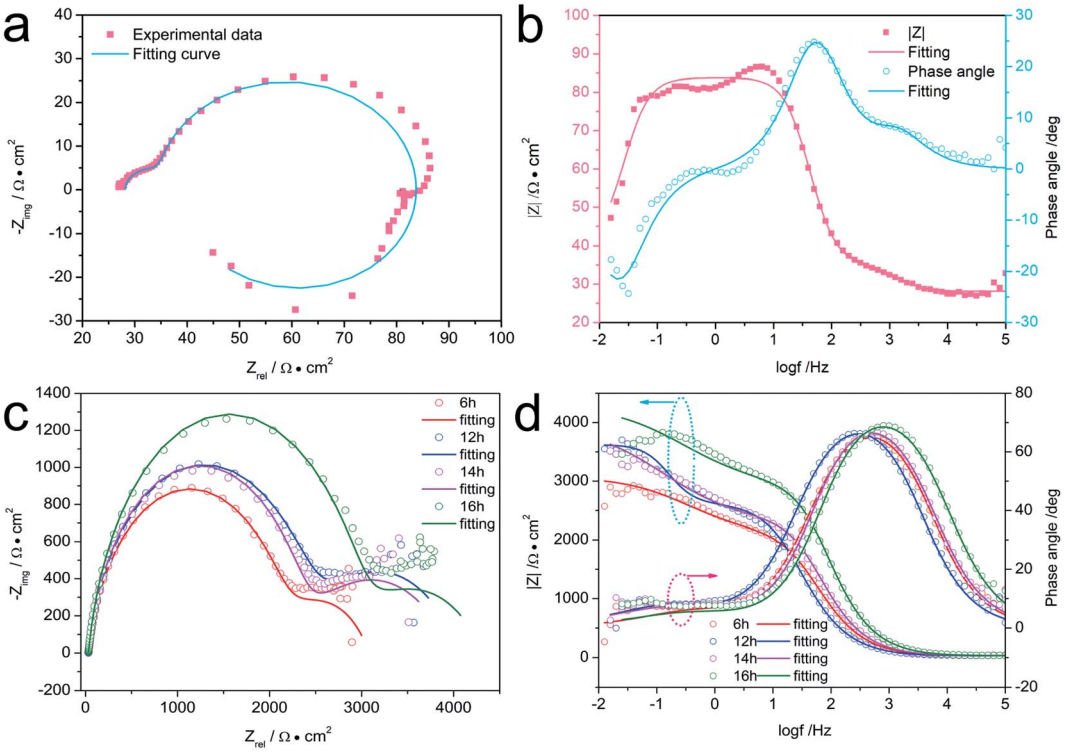

Fig. 11 EIS plots after immersion for 60 min in a 3.5 wt% NaCl solution: (a) Nyquist plots and (b) Bode plots of the untreated pure Mg sample, and (c) Nyquist plots and (d) Bode plots of the treated pure Mg samples in gaseous phase CO_2.

electrochemical double layer. Compared to the Nyquist spectrum of the untreated sample, the inductive loops completely disappear, implying that a stable nesquehonite protective film has formed on the pure Mg surface and therefore prevented corrosion.

Among the EIS characteristics of a protective film or coating on the metal surface, the low-frequency Bode impedance ($|Z|$) and the diameter of capacitive loop at high frequencies are important and useful electrochemical parameters for characterizing the corrosion resistance of the film or coating. A larger $|Z|$ or capacitive loop generally implies a better corrosion protection performance.[21] From Fig. 11, it is observed that both the capacitive loop diameter and Bode impedance $|Z|$ of the carbonated samples increase significantly compared to the pure Mg substrate and increase with the carbonation time in gaseous CO_2. This provides a demonstration of the formation of the nesquehonite protective film and its beneficial effect on the enhancement of the corrosion resistance of the pure Mg. In addition, while the maximum phase angle at the high and medium frequencies of the untreated sample is approximately 25°, the high- and medium-frequency phase angle peaks of the carbonated samples appear at approximately 70° and become broader and smoother, also proving the presence of a dense and continuous film serving as an effective barrier.

To further explain the degradation process of the Mg samples, the EIS spectra for the untreated and treated samples were fitted by two proposed equivalent electrical circuits as illustrated in Fig. 12. The untreated pure Mg sample was fitted according to the equivalent circuit presented in Fig. 12a, where R_s is the resistance of the solution between the work electrode and the reference electrode, R_{ox} and C_{ox} are the film resistance and double layer capacitance correlated with the barrier

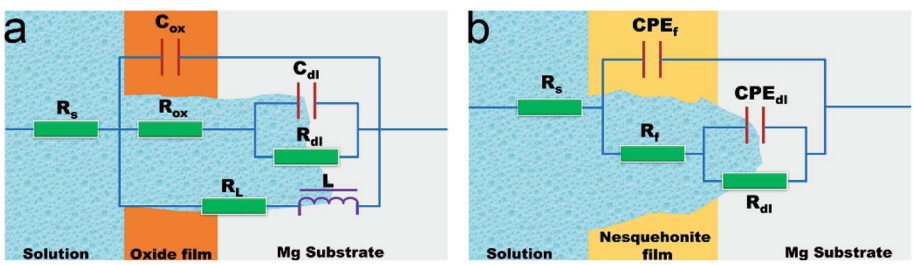

Fig. 12 Equivalent electrical circuits of (a) the untreated and (b) treated pure Mg samples in gaseous phase CO_2 after immersion for 60 min in a 3.5 wt% NaCl solution.

Table 1 EIS fitting results for the untreated pure Mg sample

R_s (Ω cm^2)	C_{ox} (F cm^{-2})	R_{ox} (Ω cm^2)	C_{dl} (F cm^{-2})	R_{dl} (Ω cm^2)	L (H cm^{-2})	R_L (Ω cm^2)	R_p (Ω cm^2)	Chi-squared
27.55	1.29×10^{-5}	9.16	8.40×10^{-5}	96.32	251.60	45.97	59.51	1.86×10^{-3}

Table 2 EIS fitting results for the carbonated pure Mg sample in gaseous phase CO_2

Time (h)	R_s (Ω cm^2)	CPE_f (Ω^{-1} s^{-n} cm^{-2})	n	R_f (Ω cm^2)	CPE_{dl} (Ω^{-1} s^{-n} cm^{-2})	n	R_{dl} (Ω cm^2)	R_p (Ω cm^2)	Chi-squared
6	31.46	3.72×10^{-6}	0.87	2152.00	7.85×10^{-4}	0.62	896.20	3048.20	1.99×10^{-3}
12	30.76	5.13×10^{-6}	0.87	2444.00	8.59×10^{-4}	0.60	1582.00	4026.00	1.17×10^{-3}
14	32.77	2.64×10^{-6}	0.90	2281.00	7.21×10^{-4}	0.55	1665.00	3946.00	1.67×10^{-3}
16	31.07	1.54×10^{-6}	0.90	2903.00	5.43×10^{-4}	0.55	1382.00	4285.00	2.10×10^{-3}

property and capacitance of the magnesium hydroxide or oxide non-protective film on the Mg surface, respectively, while R_{dl} and C_{dl} correspond to the charge transfer resistance and double layer capacitance at the Mg/electrolyte corroding interface, respectively. L and R_L represent the inductance and low-frequency loop resistance, respectively. In the equivalent circuit of the carbonated samples (Fig. 12b), R_s also represents the resistance of the solution between the work electrode and the reference electrode, and R_f and CPE_f are the corrosion resistance and constant phase element correlated with the barrier property and capacitance of the nesquehonite protective film on the Mg surface, while R_{dl} and CPE_{dl} are related to the charge transfer resistance and double layer capacitance at the Mg/electrolyte corroding interface, respectively.

The fitted EIS results of the untreated and treated samples obtained using the proposed equivalent electrical circuits are listed in Tables 1 and 2, respectively. The fitted results demonstrate that the polarization resistance ($R_p = R_f + R_{ct}$) of the carbonated pure Mg samples increases by nearly two orders of magnitude compared to that of the untreated sample. The EIS results are in good agreement with the potentiodynamic polarization curve results, further verifying that the protective nesquehonite film can offer better corrosion protection for the Mg metal.

Overall, on the basis of the electrochemical results, it can be concluded that gaseous phase CO_2 treatment can produce a highly protective nesquehonite film on pure Mg, that shields the magnesium metal from an aggressive attack by its aqueous environment.

4 Conclusions

To summarize, we developed a new environment-friendly carbonation route to *in situ* form high-corrosion-resistance nesquehonite film on pure magnesium. Analysis of XRD patterns and EDS results confirmed the formation of highly-crystalline pure nesquehonite film. Optical macrograph images and SEM micrograph images indicated that the nesquehonite film showed a continuous and compact umbrella-like structure on the pure Mg surface for carbonation times over 12 h. Electrochemical tests showed that the nesquehonite film can effectively block the corrosion of the pure Mg sample in aggressive NaCl solution. Ongoing efforts will consider the detailed formation and growth mechanism of $MgCO_3 \cdot 3H_2O$ film on pure Mg, as well as the adaptation of this method to different types of magnesium alloys.

Conflicts of interest

There are no conflicts to declare.

Acknowledgements

This work was financially supported by the Natural Science Foundation Project of Chongqing (cstc2019jcyj-msxmX0188) and Graduate Student Innovation Project of CQUST (YKJCX1820209 & YKJCX1920218).

Notes and references

1 P. Knochel, *Nat. Chem.*, 2009, **1**, 740; K. Lu, *Science*, 2010, **328**, 319; Y. Cui, S. Gao, P. Li, R. Zeng, F. Zhang, S. Li and E. Han, *Corros. Sci.*, 2017, **118**, 84; M. T. P. Prado and C. M. Cepeda-Jiménez, *Nature*, 2015, **528**, 486; J. Song, J. She, D. Chen and F. Pan, *J. Magnesium Alloys*, 2020, **8**, 1.

2 Y. Wang, B. Liu, X. Zhao, X. Zhang, Y. Miao, N. Yang, B. Yang, L. Zhang, W. Kuang, J. Li, E. Ma and Z. Shan, *Nat. Commun.*, 2018, **9**, 4058.

3 M. Esmaily, J. E. Svensson, S. Fajardo, N. Birbilis, G. S. Frankel, S. Virtanen, R. Arrabal, S. Thomas and L. G. Johansson, *Prog. Mater. Sci.*, 2017, **89**, 92; A. Atrens, G. Song, M. Liu, Z. Shi, F. Cao and M. S. Dargusch, *Adv. Eng. Mater.*, 2015, **17**, 400; R. Zeng, L. Sun, Y. Zheng, H. Cui and E. Han, *Corros. Sci.*, 2014, **79**, 69.

4 P. B. Raja and M. G. Sethuraman, *Mater. Lett.*, 2008, **62**, 113.

5 J. Gray and B. Luan, *J. Alloys Compd.*, 2002, **336**, 88; L. Li, L. Cui, R. Zeng, S. Li, X. Chen, Y. Zheng and M. B. Kannan, *Acta Biomater.*, 2018, **79**, 23; Z. Yin, W. Qi, R. Zeng, X. Chen and Y. Zheng, *J. Magnesium Alloys*, 2020, **8**, 42.

6 R. Hu, S. Zhang, J. Bu, C. Lin and G. Song, *Prog. Mater. Sci.*, 2012, **73**, 129; T. S. N. Sankara Narayanan, I. S. Park and M. H. Lee, *Prog. Mater. Sci.*, 2014, **60**, 1.
7 Y. Wang, M. Li, Y. Yang, X. Zhao, E. Ma and Z. Shan, *J. Mater. Sci. Technol.*, 2020, **44**, 48.
8 Y. Sun, J. Guo, C. Fernandez, J. Huang and Q. Peng, *Langmuir*, 2019, **35**, 300.
9 R. Lindström, J. E. Svensson and L. G. Johansson, *J. Electrochem. Soc.*, 2002, **149**, B103; M. Shahabi-Navid, M. Esmaily, J.-E. Svensson, M. Halvarsson, L. Nyborg, Y. Cao and L.-G. Johansson, *J. Electrochem. Soc.*, 2014, **161**, C277; M. Esmaily, N. Mortazavi, J. E. Svensson, L. G. Johansson and M. Halvarsson, *Ultramicro*, 2015, **153**, 45; M. Esmaily, N. Mortazavi, W. Osikowicz, H. Hindsefelt, J. E. Svensson, M. Halvarsson, G. E. Thompson and L. G. Johansson, *Corros. Sci.*, 2016, **111**, 98.
10 W. Xu, N. Birbilis, G. Sha, Y. Wang, J. E. Daniels, Y. Xiao and M. Ferry, *Nat. Mater.*, 2015, **14**, 1229.
11 D. S. Gandel, M. A. Easton, M. A. Gibson and N. Birbilis, *Mater. Chem. Phys.*, 2014, **143**, 1082.
12 D. Dwivedi, M. R. Rowles, T. Becker and K. Lepkova, *Appl. Surf. Sci.*, 2020, **509**, 9; R. A. De Motte, R. Barker, D. Burkle, S. M. Vargas, A. Neville, R. A. AF De Motte, R. Barker, D. Burkle, M. S. Vargas and A. Neville, *Mater. Chem. Phys.*, 2018, **216**, 102.
13 M. Nordsveen, S. Nesic, R. Nyborg and A. Stangeland, *Corrosion*, 2003, **59**, 443; S. Nesic and K. L. J. Lee, *Corrosion*, 2003, **59**, 616; G. Song, A. Atrens, D. Stjohn, J. Nairn and Y. Li, *Corros. Sci.*, 1997, **39**, 855.
14 G. Giester, C. L. Lengauer and B. Rieck, *Mineral. Petrol.*, 2000, **70**, 153.
15 G. W. Stephan and C. H. MacGillavry, *Acta Crystallogr., Sect. B: Struct. Crystallogr. Cryst. Chem.*, 1972, **28**, 1031.
16 M. R. Kinsolving, C. H. Macgillavry and R. Pepinsky, *Am. Mineral.*, 1950, **35**, 127; D. W. Ming and W. T. Franklin, *Soil Sci. Soc. Am. J.*, 1985, **49**, 1303.
17 M. Esmaily, J. E. Svensson, S. Fajardo, N. Birbilis, G. S. Frankel, S. Virtanen, R. Arrabal, S. Thomas and L. G. Johansson, *Prog. Mater. Sci.*, 2017, **89**, 92.
18 X. Yu and G. Li, *J. Alloys Compd.*, 2004, **364**, 193; A. J. Davenport, H. S. Isaacs and M. W. Kendig, *Corros. Sci.*, 1991, **32**, 653.
19 F. El-Taib Heakal, A. Fekry and M. Z. Fatayerji, *Electrochim. Acta*, 2009, **54**, 1545; G. T. Burstein, *Corros. Sci.*, 2005, **47**, 2858; J. Liang, P. Bala Srinivasan, C. Blawert and W. Dietzel, *Electrochim. Acta*, 2010, **55**, 6802.
20 A. D. King, N. Birbilis and J. R. Scully, *Electrochim. Acta*, 2014, **121**, 394; N. Birbilis, A. D. King, S. Thomas and G. S. Frankel, *Electrochim. Acta*, 2014, **132**, 277.
21 Q. Yao, F. Zhang, L. Song, R. Zeng, L. Cui, S. Li, Z. Wang and E. Han, *J. Alloys Compd.*, 2018, **764**, 913.